Dalton Transactions

ROYAL SOCIETY OF CHEMISTRY

COMMUNICATION

View Article Online
View Journal | View Issue

Cite this: *Dalton Trans.*, 2026, **55**, 2041

Received 3rd December 2025,
Accepted 14th January 2026

DOI: 10.1039/d5dt02896e

rsc.li/dalton

Substituent effect on the boron atoms in boron-bridged hexazenes

Masahiro Yamamoto and Makoto Yamashita *

This work investigates the substituent effect on the boron atom toward the electronic structure and optical properties of boron-bridged hexazene derivatives (B_2N_6). DFT studies revealed that the substituents on the boron atom strongly affect the energy level of the N_6-centered π system and alter the absorption/emission spectra. In addition, cyclic voltammetry demonstrates the electron-accepting character of the B_2N_6 scaffold.

π-Conjugated molecules bridged by a four-coordinate boron centre with an *N*,*N*′-chelate, such as BODIPY derivatives (Fig. 1a), exhibit characteristic optical and electronic properties.[1,2] The bridging boron atoms fix the planarity of the π-conjugated framework, and the properties of these molecules can be tuned by changing the substituents on the boron atom.[3–5] Similarly, boron-bridged nitrogen-rich π-conjugated systems, such as triazene **I**,[6] formazanate **II**,[7–13] and 1,2-bis((1*H*-pyrrol-2-yl)methylene)hydrazine **III**,[14] also display emission and redox behavior upon boron bridging, indicating that this boron-bridging strategy can expand the scope of nitrogen-linked π-systems.

Compounds containing catenated nitrogen atoms are generally unstable due to lone-pair repulsion and the tendency to release thermodynamically stable N_2.[15,16] One of the limited isolable examples of such a polynitrogen π system is metal-bridged hexazene (M_2N_6), where π-conjugated consecutive six nitrogen atoms are stabilized by two metal centres (Fig. 1b). These metal-bridged hexazenes are formed through the reductive coupling of organic azides by low-oxidation-state metal reagents. Following the initial iron examples,[17–20] related Mg-,[21,22] Mg/Be-,[23] Zn-,[24–28] and In/Zn-[29] mediated reactions have been reported, and the subsequent transmetallation provides access to Li/Zn- and Al_2-containing analogues.[25,26] A digermane bearing (dialkylalumanyl)alkenyl groups also affords an Al_2N_6 species upon reaction with aryl azides.[30] Recent studies further show that hexazenes can appear as reactive intermediates in catalytic ammonia oxidation, as demonstrated by the isolation of a diruthenium–hexazene complex.[31] Despite these advances, the optical and electronic properties of metal-bridged hexazenes remain unknown.

We recently reported the synthesis of boron-bridged hexazenes (B_2N_6) through the reaction of tetra(*o*-tolyl)diborane(4)[32] with organic azides (Fig. 1c).[33] These compounds feature a planar bicyclic B_2N_6 core consisting of a conjugated N_6 chain and two bridging boron atoms. Remarkably, these B_2N_6 compounds are bench-stable and strongly fluorescent with quantum yields of up to 96%, in contrast to the non-emissive M_2N_6 complexes.[17–31] However, the influence of substituents at the boron atoms on the structure and properties of the B_2N_6 framework has not yet been clarified. Herein, we report the synthesis of B_2N_6 derivatives having triflate, chloro, and methyl groups on the boron atoms and their properties using X-ray crystallography, photophysical and electrochemical measurements, and DFT calculations to reveal the substituent effect on the boron atom toward the electronic structure and the properties of these N_6 π-systems.

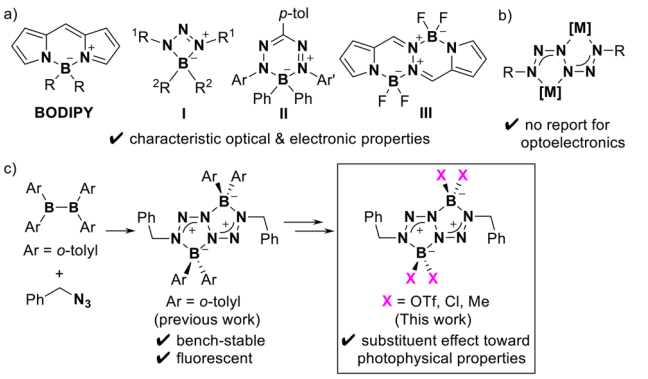

Fig. 1 (a) Examples of boron-bridged conjugated systems with an *N*-chelate, (b) metal-bridged hexazenes, and (c) boron-bridged hexazenes.

Department of Chemistry, School of Science, Institute of Science Tokyo, 2-12-1, Ookayama, Meguro-ku, Tokyo, 152-8551 Japan.
E-mail: yamashita.m.6dbb@m.isct.ac.jp

The previously reported B_2N_6 molecule **1**[33] bearing tolyl groups at the boron atoms was treated with four equivalents of trifluoromethanesulfonic acid to afford the corresponding tetra(triflate) derivative **2** (Scheme 1). Notably, the B_2N_6 core was not decomposed by the treatment with a strong acid, TfOH, implying the high stability of the B_2N_6 scaffold toward Brønsted acids. Subsequent treatment of **2** with four equivalents of $^nBu_4NCl$ furnished the tetra(chloro) derivative **3** through a ligand exchange between triflate and chloride anions. The reaction of **2** with four equivalents of $AlMe_3$ led to the formation of tetra(methyl) derivative **4**. **4** was also able to be synthesized from the chloro derivative **3** by a treatment with a methyl Grignard reagent. Note that these compounds can be handled under air at room temperature.

Single-crystal X-ray diffraction analysis was performed to determine the crystal structures of **2**, **3**, and **4** (Fig. 2). Compared with the previously reported **1** [N1–N2: 1.296(1) Å, N2–N3: 1.289(2) Å],[33] the N1–N2 [**2**: 1.302(3) Å, **3**: 1.301(2) Å, **4**: 1.299(2) Å] and N2–N3 [**2**: 1.286(3) Å, **3**: 1.298(2) Å, **4**: 1.290(2) Å] bond lengths show no significant differences among them regardless of the substituent on the boron atom and are slightly longer than the typical N=N double bond (*ca.* 1.25 Å).[34] The central N3–N3* bonds [**2**: 1.398(2) Å, **3**: 1.382(3) Å, **4**: 1.392(3) Å] are slightly shorter than a typical N–N single bond (*ca.* 1.45 Å),[34] being similar to that of **1** [1.401(2) Å].[33] These observations indicate that substitution at the boron atom does not significantly alter the structure of the B_2N_6 framework and that the eight π electrons in these derivatives are delocalized over the six nitrogen atoms through two triazaallyl-type resonance structures.

Next, the absorption and emission spectra of each B_2N_6 molecule in dichloromethane were obtained (Fig. 3, Table 1). In comparison to **1**,[33] **4** exhibited a slightly blue-shifted absorption and emission with an absorption maximum at 409 nm and an emission maximum at 495 nm, respectively, while **3** displayed a further blue-shifted absorption and emission. The triflate derivative **2** has an absorption maximum at 354 nm and shows no detectable emission. Thus, introduction of electron-withdrawing substituents such as **3** or **2** results in a blue-shift for the absorption. Among four compounds, **1**, **3**, and **4** showed clear vibronic structures in both absorption and emission spectra, likely due to their relatively rigid molecular frameworks. In contrast, **2** displayed a broad absorption devoid of vibronic features, reflecting a relatively large degree of molecular freedom and an increased relaxation rate for the excited state associated with the OTf groups. We also examined

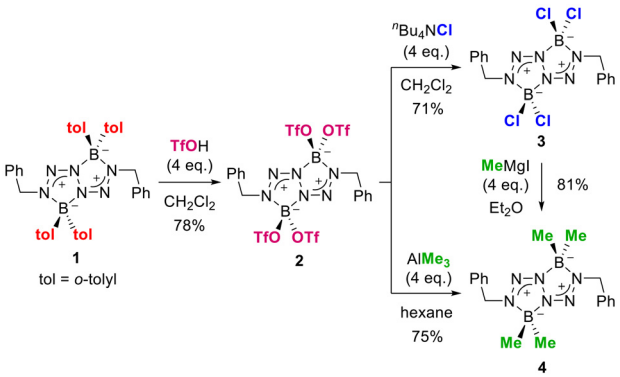

Scheme 1 Synthesis of **2**, **3**, and **4**.

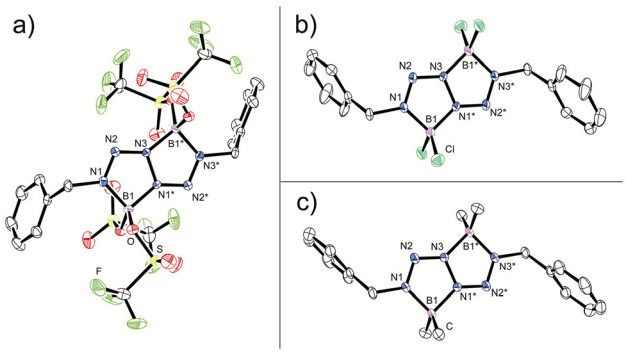

Fig. 2 Molecular structures of (a) **2**, (b) **3**, and (c) **4** [ellipsoids set at 50% probability, hydrogen atoms omitted for clarity, one of two independent molecules for **2**].

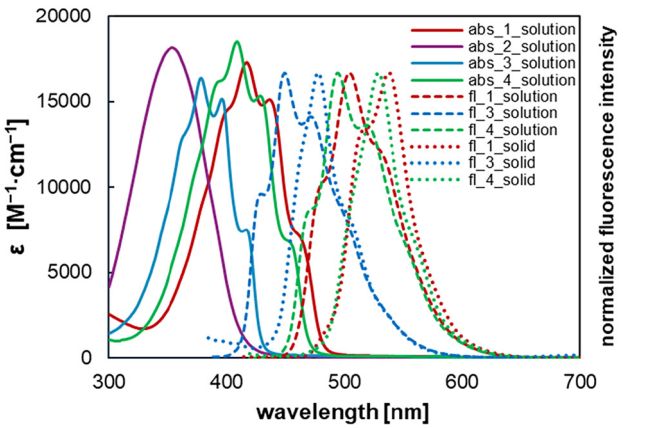

Fig. 3 UV-vis absorption (solid lines) and normalized emission (dashed lines) spectra of **1**,[33] **2**, **3**, and **4** in dichloromethane (50 μM) and normalized emission in the solid state (chain line).

Table 1 UV-vis absorption and fluorescence properties of **1**,[33] **2**, **3**, and **4**

cpd	State	λ_{abs} [a] [nm]	ε [10^4 M^{-1} cm^{-1}]	λ_{em} [b] [nm]	τ [ns]	Φ_{fl} [c] [%]
1[33]	Solution[d]	418	1.73	504	7.9	88.6
2	Solution[d]	354	1.81	—	—	—
3	Solution[d]	379	1.64	450	<0.1	1.5
4	Solution[d]	409	1.84	495	6.2	82.4
1[33]	Solid	—	—	538	—	52.1
3	Solid	—	—	478	—	26.7
4	Solid	—	—	529	—	74.0

[a] The wavelength of the largest molar absorption coefficient. [b] The wavelength of the brightest emission maximum. [c] Determined with a calibrated integrating sphere. [d] In dichloromethane (50 μM).

the effect of solvent polarity on the absorption of **2** (Fig. S17), based on the hypothesis that it might shift the equilibrium, including the dissociation of the triflate from the boron center, potentially affecting the absorption wavelength. However, we observed no significant changes across a series of different solvents (hexane, toluene, CH_2Cl_2, CH_3CN, and ethanol), including coordinating solvents such as CH_3CN. This suggests that the dissociation equilibrium is minimal and likely has little to no influence on the absorption behavior of **2**. It should be noted that the trial to replace the chloride in **3** with $AgPF_6$ afforded an unidentified compound possessing a B–F bond as judged from the ^{11}B and ^{19}F NMR spectra. **3** and **4** exhibit fluorescence in the solid state. In particular, for the chloro-derivative **3**, the fluorescence quantum yield increases from 1.5% in solution to 26.7% in the solid state. This enhancement can be attributed to the suppression of non-radiative decay in the solid state. Consistent with this view, the emission lifetime in solution is very short (<0.1 ns), likely due to rapid non-radiative decay.

To better understand the difference in optical features, DFT calculations were performed [B3LYP/6-31+G(d) with the SMD solvation model (dichloromethane)]. The characteristic molecular orbitals are summarized in the order of increasing energy gap for the main absorptions (Fig. 4). In the previously

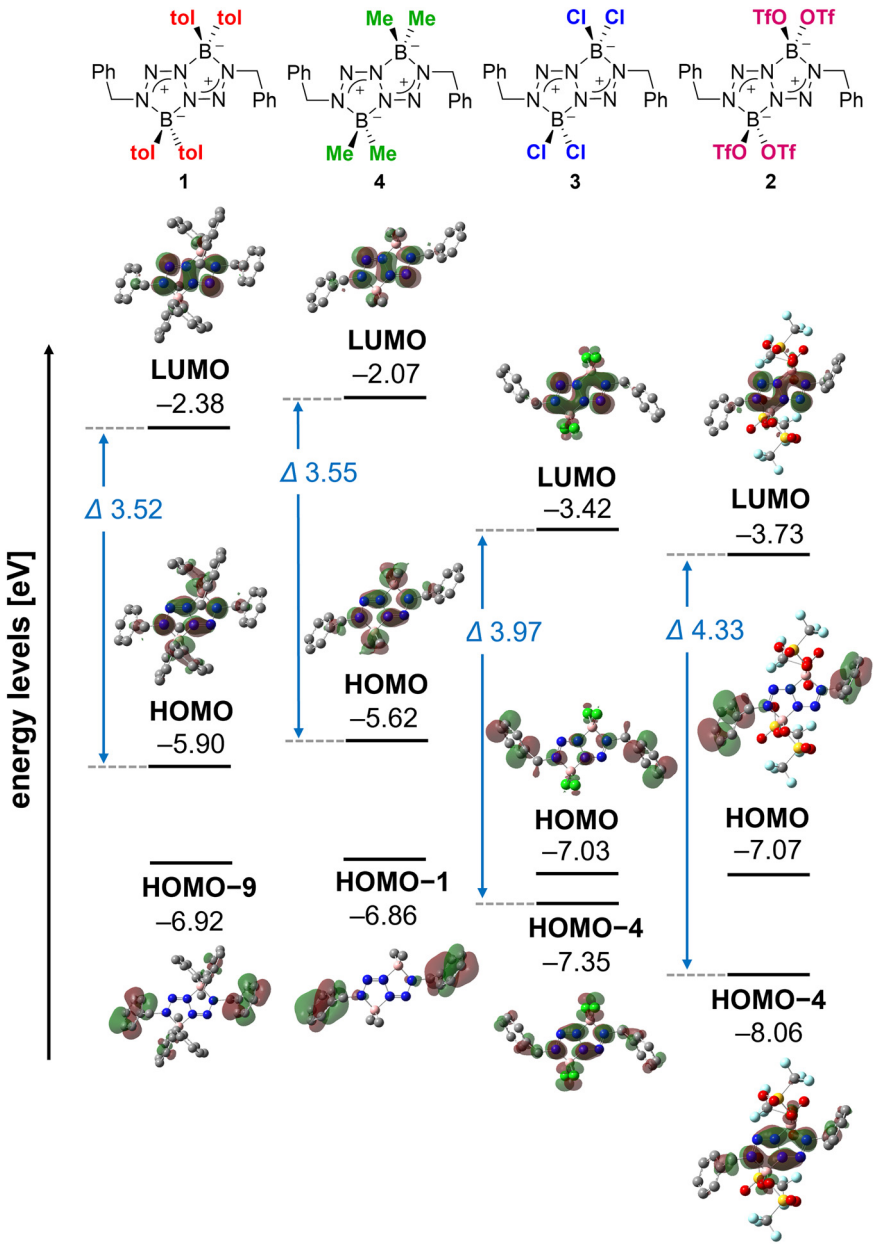

Fig. 4 Energy profiles and frontier orbitals of **1**,[33] **4**, **3**, and **2** calculated at the B3LYP/6-31+G(d) level of theory with the SMD solvation model of dichloromethane (hydrogen atoms are omitted for clarity).

reported **1**,[33] the HOMO is mainly composed of the π orbitals of the N_6 unit with some contribution from the B–C σ bond, whereas the LUMO is primarily localized on the N_6-centered π* orbitals. TD-DFT calculations indicated that the absorption in the visible region predominantly originates from the HOMO–LUMO transition (3.52 eV; f = 0.3456). In the case of **4**, both the N_6-based HOMO and LUMO were raised compared to those of **1**, probably due to the σ-donating effect of the methyl groups. Thus, replacing the tolyl groups with methyl groups would contribute less effectively to the HOMO, leading to the slightly larger HOMO–LUMO gap and the blue-shifted absorption in **4**. Introduction of Cl substituents lowered the N_6-related orbitals in **3** [LUMO and HOMO−4], reflecting the σ-accepting inductive effect of chloride. Due to the lowering of the N_6-related orbitals, the π-orbitals of the benzyl group became the HOMO in **3**. TD-DFT calculations showed that the major absorption of **3** is based on the transition from HOMO−4 to the LUMO (3.97 eV, 360 nm, f = 0.3870), while the transition from the HOMO to the LUMO is less contributing with smaller oscillator strengths. In the case of **2**, the stronger σ-accepting inductive effect of the triflate lowered the HOMO and LUMO further. However, similar to **3**, the absorption is mainly contributed by the transition from HOMO−4 to the LUMO (4.33 eV; 323 nm f = 0.4243).

To determine the electron-accepting properties of the B_2N_6 derivatives, cyclic voltammetry (CV) was performed in dichloromethane, using the oxidation of ferrocene as an external reference (Fig. 5). The electrochemical measurement in the present study revealed that **1** and **4** exhibited quasi-reversible reduction waves, with half-wave potentials of −1.81 V and −2.05 V, respectively. This result indicates that the B_2N_6 unit exhibits electron-accepting character due to the existence of the N_6-conjugated π-system. In contrast, **2** and **3** displayed only irreversible reduction waves (Fig. S18 and S19), suggesting that the reduced species are unstable. This instability is likely due to cleavage of the B–E bonds (E = O, Cl) upon injection of an electron to the σ*(B–E) orbital in the LUMO. The lower negative reduction potential of **4** (−2.15 V) (Fig. 5) and higher reduction potential of **3** (−0.79 V) and **2** (−0.29 V) (Fig. S18 and S19) compared to that of **1** (−1.92 V) (Fig. 5) reflect the higher-lying LUMO level of **4** (−2.07 eV) and lower-lying that of **3** (−3.42 eV) and **2** (−3.73 eV) than that of **1** (−2.38 eV) predicted by the DFT calculations (Fig. 4).

In summary, modifying the boron substituents of the B_2N_6 framework enables tuning of the energy levels of the N_6-centred π orbitals, thereby altering the optical spectra. Cyclic voltammetry measurements revealed quasi-reversible reduction waves for the tolyl and methyl derivatives, indicating that the B_2N_6 core exhibits electron-accepting character. Further investigation of the properties of the N_6-π systems is ongoing with additional derivatization of the B_2N_6 framework.

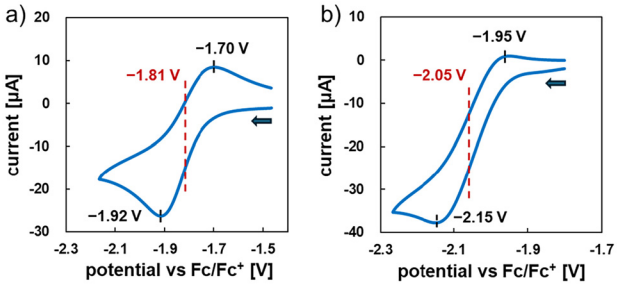

Fig. 5 Cyclic voltammetry of (a) **1**[33] and (b) **4** in dichloromethane (2 mM).

Conflicts of interest

There are no conflicts to declare.

Data availability

The data supporting this article have been included in the supplementary information (SI). Supplementary information is available. See DOI: https://doi.org/10.1039/d5dt02896e.

CCDC 2512981–2512983 contain the supplementary crystallographic data for this paper.[35a–c]

Acknowledgements

This research was supported by a Grant-in-Aid for Scientific Research (A) (24H00455 for M. Yamashita), a Grant-in-Aid for Transformative Research Areas "Condensed Conjugation" (23H04022 for M. Yamashita). M. Yamamoto is grateful to the Transformative Research Area "Condensed Conjugation" for the fellowship for junior scientists and a Grant-in-Aid for JSPS Fellows (24KJ1265). We thank Prof. H. Shinokubo and Prof. N. Fukui at Nagoya University and Prof. G. Fukuhara and Prof. Y. Sagara at the Institute of Science Tokyo for providing access to instruments for the measurement of fluorescence quantum yields and lifetimes. Computations were performed using the Research Center for Computational Science, Okazaki, Japan (25-IMS-C005).

References

1 A. Loudet and K. Burgess, *Chem. Rev.*, 2007, **107**, 4891–4932.
2 N. A. Bumagina, E. V. Antina, A. A. Ksenofontov, L. A. Antina, A. A. Kalyagin and M. B. Berezin, *Coord. Chem. Rev.*, 2022, **469**, 214684.
3 E. Bodio and C. Goze, *Dyes Pigm.*, 2019, **160**, 700–710.
4 N. Boens, B. Verbelen, M. J. Ortiz, L. Jiao and W. Dehaen, *Coord. Chem. Rev.*, 2019, **399**, 213024.
5 R. L. Gapare and A. Thompson, *Chem. Commun.*, 2022, **58**, 7351–7359.
6 A. A. Suleymanov, R. Scopelliti and K. Severin, *Inorg. Chem.*, 2022, **61**, 1546–1551.

7 R. R. Maar, S. M. Barbon, N. Sharma, H. Groom, L. G. Luyt and J. B. Gilroy, *Chem. – Eur. J.*, 2015, **21**, 15589–15599.
8 R. R. Maar, R. Zhang, D. G. Stephens, Z. Ding and J. B. Gilroy, *Angew. Chem., Int. Ed.*, 2019, **58**, 1052–1056.
9 F. L. Buguis, R. R. Maar, V. N. Staroverov and J. B. Gilroy, *Chem. – Eur. J.*, 2021, **27**, 2854–2860.
10 R. R. Maar, B. D. Katzman, P. D. Boyle, V. N. Staroverov and J. B. Gilroy, *Angew. Chem., Int. Ed.*, 2021, **60**, 5152–5156.
11 H. Xiang, L. Zhao, L. Yu, H. Chen, C. Wei, Y. Chen and Y. Zhao, *Nat. Commun.*, 2021, **12**, 218.
12 B. D. Katzman, R. R. Maar, D. Cappello, M. O. Sattler, P. D. Boyle, V. N. Staroverov and J. B. Gilroy, *Chem. Commun.*, 2021, **57**, 9530–9533.
13 J. B. Gilroy and E. Otten, *Chem. Soc. Rev.*, 2020, **49**, 85–113.
14 A. N. Bismillah and I. Aprahamian, *Chem. Soc. Rev.*, 2021, **50**, 5631–5649.
15 Y. Qu and S. P. Babailov, *J. Mater. Chem. A*, 2018, **6**, 1915–1940.
16 O. T. O'Sullivan and M. J. Zdilla, *Chem. Rev.*, 2020, **120**, 5682–5744.
17 R. E. Cowley, J. Elhaïk, N. A. Eckert, W. W. Brennessel, E. Bill and P. L. Holland, *J. Am. Chem. Soc.*, 2008, **130**, 6074–6075.
18 R. E. Cowley, N. J. DeYonker, N. A. Eckert, T. R. Cundari, S. DeBeer, E. Bill, X. Ottenwaelder, C. Flaschenriem and P. L. Holland, *Inorg. Chem.*, 2010, **49**, 6172–6187.
19 J. A. Bellow, P. D. Martin, R. L. Lord and S. Groysman, *Inorg. Chem.*, 2013, **52**, 12335–12337.
20 L. Fohlmeister, C. Jones, L. Fohlmeister and C. Jones, *Aust. J. Chem.*, 2014, **67**, 1011–1016.
21 S. J. Bonyhady, S. P. Green, C. Jones, S. Nembenna and A. Stasch, *Angew. Chem., Int. Ed.*, 2009, **48**, 2973–2977.
22 S. J. Bonyhady, C. Jones, S. Nembenna, A. Stasch, A. J. Edwards and G. J. McIntyre, *Chem. – Eur. J.*, 2010, **16**, 938–955.
23 C. Berthold, J. Maurer, L. Klerner, S. Harder and M. R. Buchner, *Angew. Chem., Int. Ed.*, 2024, **63**, e202408422.
24 S. Gondzik, S. Schulz, D. Bläser, C. Wölper, R. Haack and G. Jansen, *Chem. Commun.*, 2013, **50**, 927–929.
25 S. Gondzik, C. Wölper, R. Haack, G. Jansen and S. Schulz, *Dalton Trans.*, 2015, **44**, 15703–15711.
26 C. Stienen, S. Gondzik, A. Gehlhaar, R. Haack, C. Wölper, G. Jansen and S. Schulz, *Organometallics*, 2016, **35**, 1022–1029.
27 B. Li, K. Huse, C. Wölper and S. Schulz, *Chem. Commun.*, 2021, **57**, 13692–13695.
28 S. Xu, S. Jiang and Z. Xu, *Polyhedron*, 2023, **242**, 116525.
29 M. D. Anker, Y. Altaf, M. Lein and M. P. Coles, *Dalton Trans.*, 2019, **48**, 16588–16594.
30 W. Uhl, C. Honacker, N. Lawrence, A. Hepp, L. Schürmann and M. Layh, *Z. Anorg. Allg. Chem.*, 2018, **644**, 945–955.
31 S. Feng, J. Chen, R. Wang, H. Li, J. Xie, Z. Guo, T. Lau and Y. Liu, *J. Am. Chem. Soc.*, 2024, **146**, 21490–21495.
32 N. Tsukahara, H. Asakawa, K.-H. Lee, Z. Lin and M. Yamashita, *J. Am. Chem. Soc.*, 2017, **139**, 2593–2596.
33 M. Yamamoto, W. C. Chan, Z. Lin and M. Yamashita, *Chem. – Eur. J.*, 2023, **29**, e202302027.
34 J. Emsley, *The elements*, Clarendon Press Oxford University Press, Oxford, 3rd edn, 1998.
35 (*a*) CCDC 2512981: Experimental Crystal Structure Determination, 2026, DOI: 10.5517/ccdc.csd.cc2qbyxy; (*b*) CCDC 2512982: Experimental Crystal Structure Determination, 2026, DOI: 10.5517/ccdc.csd.cc2qbyyz; (*c*) CCDC 2512983: Experimental Crystal Structure Determination, 2026, DOI: 10.5517/ccdc.csd.cc2qbyz0.